

Received July 17, 2021, accepted August 8, 2021, date of publication August 11, 2021, date of current version August 23, 2021.

Digital Object Identifier 10.1109/ACCESS.2021.3104030

# Fuzzy Multiple Hidden Layer Neural Sliding Mode Control of Active Power Filter With Multiple Feedback Loop

JIE ZHUO<sup>1</sup>, CUICUI AN<sup>2</sup>, AND JUNTAO FEI<sup>1,2,3</sup> (Senior Member, IEEE)

<sup>1</sup>College of IoT Engineering, Hohai University, Changzhou 213022, China

<sup>2</sup>College of Mechanical and Electrical Engineering, Hohai University, Changzhou 213022, China

<sup>3</sup>Jiangsu Key Laboratory of Power Transmission and Distribution Equipment Technology, Changzhou 213022, China

Corresponding author: Juntao Fei (jtfei@hhu.edu.cn)

This work was supported in part by the National Science Foundation of China under Grant 61873085.

**ABSTRACT** A fuzzy multiple hidden layer neural sliding mode control with multiple feedback loop (FMHLNSMCMFL) is proposed for a single-phase active power filter (APF), where a sliding mode controller is designed to make the current tracking error converge to zero and a new neural network with multiple feedback loops is introduced to approximate unknown dynamics. At the same time, the fuzzy neural network can eliminate chattering, improve the control accuracy and reduce the current distortion rate of APF. Moreover, the proposed double feedback fuzzy double hidden layer recurrent neural network is the weighted sum of fuzzy network and double hidden layer network and has strong global learning ability. The adaptive parameters obtained by Lyapunov function can ensure the asymptotic stability of the system. Simulation and hardware experiments verify the introduced FMHLNSMCMFL scheme is a viable control solution for the APF.


**INDEX TERMS** Fuzzy multiple hidden layer neural sliding mode control, multiple feedback loop, sliding mode control, active power filter.

## I. INTRODUCTION

In recent years, power electronics technology has been widely used in power systems. However, with the continuous increase of the nonlinear load in power electronic equipments, power quality distortion has become a serious problem [1]–[4]. Power grid harmonic control has always attracted the attention of many scholars. APF can dynamically filter out the harmonics in the system, and completely absorb the harmonics in the system without resonance. The key principle of APF to eliminate harmonics is to control the on-off time of IGBTs [5]–[7]. Sliding mode control is the mainstream algorithm for harmonic control in APF because of its rapidity and strong robustness [8]–[11]. Haghghi and Ziaratban [12] studied a non-integer sliding mode controller to stabilize fractional-order nonlinear systems. Pashaei and Badamchizadeh [13] presented a new fractional-order sliding mode controller for disturbance rejection and stabilization of a class of fractional-order systems with

mismatched disturbances. Ding *et al.* [14] proposed a non-singular fast fixed-time sliding surface for a flexible air-breathing hypersonic vehicle. Mohammad *et al.* [15] proposed a novel speed-control scheme for switched reluctance motor drive based on a fast terminal sliding mode control method. Safa *et al.* [16] defined a new sliding surface by combining the conventional sliding surface in terminal sliding mode control and the nonlinear function of the system state integral. Although sliding mode control can ensure the stability of the system under unknown disturbances and model uncertainties, it cannot avoid the chattering. In order to solve the above problems and eliminate the chattering, neural network can be used to approach the system nonlinearities to increase the accuracy of the control algorithm.

Nowadays, intelligent algorithms including fuzzy control, neural network control have been applied to APF. Feedforward neural network (such as radial basis function (RBF) neural network) has become a research hotspot in the field of intelligent control due to its excellent approximation characteristics. Although the feedforward neural network has poor dynamic characteristics, it has the characteristics of simple

The associate editor coordinating the review of this manuscript and approving it for publication was Valentina E. Balas .

structure and wide application range. Zhang and Liu [17] proposed an adaptive radical basis function neural network to deal with dynamic tracking error problems for a three-phase APF. Safa et al. [18] combined the state feedback controller and the terminal sliding mode controller into a fuzzy system. Vali et al. [19] proposed an adaptive neural sliding mode control based on RBF neural network approximation to eliminate chattering phenomenon in the sliding mode controller. Fu and Li [20] designed a recurrent neural network control method for single-phase grid-connected converters with LCL filters. Terminal sliding mode controller with new neural network structure and intelligent global sliding mode controller with feature selection neural network and fuzzy neural networks are proposed for active power filters in [21]–[24].

The universal approximation theorem indicates that the fuzzy system is a new universal approximator in addition to polynomial function approximators and neural network approximators. Fuzzy neural network (FNN) is a popular technology combining the knowledge expression ability of fuzzy logic system with the powerful self-learning ability of neural network [25]. In [26], a novel adaptive fuzzy hysteresis band controller is proposed for a current control system. In [27], a fuzzy neural network estimator is used to estimate the upper bound of the error between the actual value and the observed value of the disturbance, which greatly improves the control accuracy. In [28], a 5/5 fuzzy rule implementation in a fuzzy controller conjunction with an indirect control technique is proposed to improve power quality. Several fuzzy and neural network methods to approximate the sliding mode controller and system nonlinearities are investigated for active power filters and other dynamic systems in [29]–[33].

Motivated by the research methods above, a FMHLNSMCMFL scheme is proposed to approximate the nonlinear term and eliminate the chattering and then improve the harmonic suppression. Compared with existing methods, the contributions of the proposed controller are summarized as:

(1) A FMHLNSMCMFL approximator that combines the advantages of the recurrent neural network and the fuzzy neural network, and has a strong global learning ability is proposed. The two hidden layers enhance the feature extraction capabilities of the neural network. The dual feedback combines the current time and the output value of the previous time neuron to improve the stability of the system.

(2) Because the existence of the activation function of the hidden layer can make the neural network have a strong fitting function and training accuracy, the introduction of double hidden layers can enable the neural network to achieve more complex function fitting and provide higher training accuracy. Using a double hidden layer neural network to replace a single hidden layer neural network can reduce the number of nodes correspondingly and increase the response speed while maintaining the same accuracy.

(3) The proposed neural network phase also has a double feedback structure to further improve the approximation

ability compared with conventional neural networks. The existence of internal feedback and external feedback can make the system make self-adjustment in combination with the state information and output signal at the previous moment, making the output of the system smoother and preventing sudden changes.

This paper is organized as follows. In Section 2, the principle of a single-phase APF is given. Section 3 introduces a new neural network, FMHLNSMCMFL, is introduced, and the stability of the system is proved. In Section 4, the effectiveness of the method is verified by MATLAB simulation. Section 5 designs the hardware experiment. Section 7 gives the conclusion.

## II. DYNAMIC MODEL OF ACTIVE POWER FILTER AND PROBLEM FORMULATION

APF is more and more widely used in dealing with harmonic, such as Non-ferrous metallurgy, Electrified railway, and Petrochemical industry. The main circuit of a single APF is composed of four power electronic devices and DC-side capacitors. The working principle of APF is to collect the corresponding current and voltage signal through the sensor, and then send them to the controller. Finally, the output signal of the controller is modulated into pulse width modulation (PWM), and the IGBT Driver receives the modulated signal pulse signal.

Fig.1 is the block diagram of the APF control system,  $U_s$  and  $U_{dc}$  are a supply voltage and a DC link voltage.  $i_s$  is a grid current,  $i_c$  is a compensation current and  $i_L$  is a load current.  $L$  and  $R$  are the equivalent inductance and resistance values of the AC side.

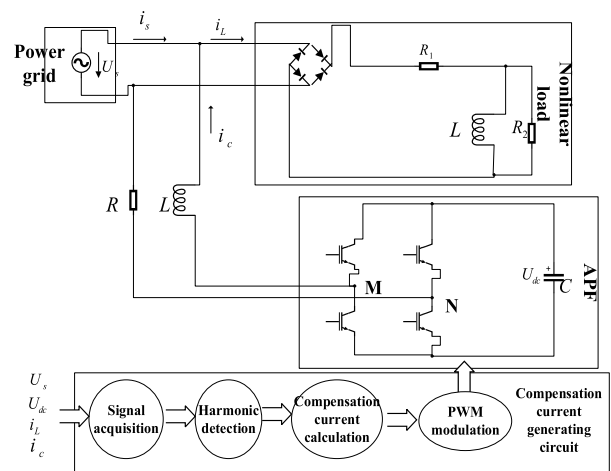


FIGURE 1. The block diagram of active power filter.

Assuming that the IGBTs used in the control system is ideal, a switching function is defined as:

$$U = \begin{cases} 1, & VT1, VT4 \text{ on, } VT2, VT3 \text{ off} \\ -1, & VT1, VT4 \text{ off, } VT2, VT3 \text{ on} \end{cases} \quad (1)$$

According to Kirchhoff voltage and current laws, the equation of compensation current in the main circuit is obtained as:

$$\dot{i}_c = -\frac{R}{L}i_c + \frac{1}{L}U_s - \frac{1}{L}U_{MN} \quad (2)$$

where  $U_{MN} = U \cdot U_{dc}$  is a AC-side voltage. The derivative of (2) can be derived as:

$$\ddot{i}_c = \frac{R^2}{L^2}i_c - \frac{R}{L^2}U_s + \frac{1}{L}\dot{U}_s + (\frac{R}{L^2}U_{dc} - \frac{1}{L}\dot{U}_{dc}) \cdot U \quad (3)$$

Therefore, the second order model of the system can be obtained as:

$$\ddot{x} = f(x) + bu + d(t) \quad (4)$$

where  $x$  is the compensation current  $i_c$  and control variable  $u = U$ , and  $d(t)$  is a continuous differentiable and unknown external disturbance,

$$f(x) = \frac{R^2}{L^2}i_c - \frac{R}{L^2}U_s + \frac{1}{L}U_s \quad (5)$$

$$b = \frac{R}{L^2}U_{dc} - \frac{1}{L}\dot{U}_{dc} \quad (6)$$

We can assume  $d(t)$  is a continuous bounded function as:  $0 < d(t) < D, D > 0$ .

The objective of the APF control system is to design a current controller to make the harmonic compensation current track a reference current.

The tracking error is defined as:

$$e = x - x_r \quad (7)$$

where  $x_r$  is a reference current.

The first derivative of tracking error is:

$$\dot{e} = \dot{x} - \dot{x}_r \quad (8)$$

Then, a standard sliding surface is defined as:

$$s = ce + \dot{e} \quad (9)$$

where  $c$  is a sliding surface parameter

Thus, the first derivative of the sliding surface is:

$$\dot{s} = c\dot{e} + \ddot{e} \quad (10)$$

Ignoring the disturbance  $d(t)$  and setting  $\dot{s} = 0$  to solve the equivalent control term  $u_{eq}$  as:

$$u_{eq} = -\frac{1}{b}[-\ddot{x}_r + c\dot{e} + f(x)] \quad (11)$$

A switching term is added to compensate the disturbance and make the control system stable:

$$u_{sw} = -\frac{1}{b}K_w \text{sgn}(s) \quad (12)$$

where  $K_w$  is a sliding gain.

Therefore, a comprehensive controller is proposed as:

$$\begin{aligned} u &= u_{eq} + u_{sw} \\ &= -\frac{1}{b}[-\ddot{x}_r + c\dot{e} + f(x) + K_w \text{sgn}(s)] \end{aligned} \quad (13)$$

**Theorem 1:** Considering the nonlinear mathematical model (6), if we choose the controller (13), the asymptotic stability of APF control system can be guaranteed.

$$\dot{V} = \frac{1}{2}\dot{s}^2 \quad (14)$$

By substituting (10) and (13) into the first derivative of (14), we can obtain:

$$\begin{aligned} \dot{V} &= s[c\dot{e} + f(x) + bu + d(t) - \ddot{x}_r] \\ &= s[c\dot{e} + f(x) + b\{-\frac{1}{b}[-\ddot{x}_r + c\dot{e} + f(x) + K_w \text{sgn}(s)]\} \\ &\quad + d(t) - \ddot{x}_r] \\ &= s(d(t) - K_w \text{sgn}(s)) = sd(t) - K_w |s| \\ &\leq |s|D - K_w |s| \leq -|s|(K_w - D) \end{aligned} \quad (15)$$

If  $K_w > D$ ,  $\dot{V} \leq 0$  is guaranteed, which is negative semidefinite, that is, the system can reach the designed sliding surface and remain on the sliding surface. According to Barbalat's Lemma and its deductions, the system is asymptotically stable and the tracking error and sliding surface can converge to zero asymptotically.

### III. FUZZY MULTIPLE HIDDEN LAYER NEURAL SLIDING MODE CONTROL WITH MULTIPLE FEEDBACK LOOP

However the ideal controller (13) depends on an accurate mathematical model, it cannot be realized if  $f(x)$  is unknown. Therefore, in this part, a FMHLNSMCMFL strategy is proposed to approximate the unknown  $f(x)$ .

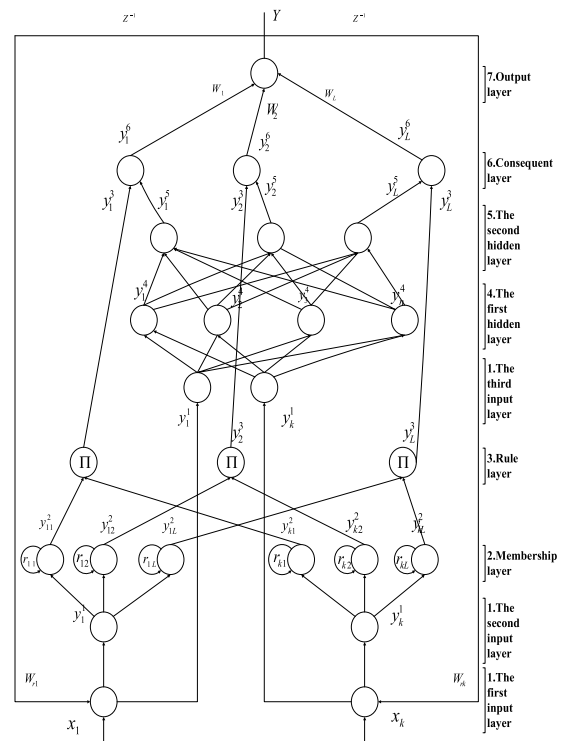


FIGURE 2. The block diagram of DFFDHLRNN.

### A. STRUCTURE OF FMHLNSMCMFL

The universal approximation theorem indicates that the fuzzy neural network and the feedforward neural network are both good nonlinear approximators. The proposed DFFDHLRNN is a weighted summation of the output of the FNN and the multiple hidden layer neural network, which makes the approximation error smaller and the approximation accuracy higher. The structure of DFFDHLRNN is shown in Fig. 2. It consists of 7 layers: an input layer, a membership layer, a rule layer, two hidden layers, a consequent layer, and an output layer. The signal transmission of DFFDHLRNN and the basic function of each layer are introduced in the following steps:

**Layer 1- Input layer:** It is also divided into three layers: the first, the second and the third input layers. The first input layer is the input part of the whole neural network where the completed work is to input the signal of the neural network and accept the output of the neural network in the last iteration process through the feedback weight  $W_{eq}$ . The second input layer is the input layer of fuzzy neural network, which completes the signal transmission of the upper part. The third input layer is the input layer of double hidden layer, used to complete the signal transmission of the upper part. In this paper, the output of the  $i$ -th node of the first input layer can be described as:

$$y_i^1 = x_i \cdot exY \cdot W_{ri} \quad (16)$$

where  $y_i^1$  represents the output value of the  $i$ -th node of the first layer neural network and  $exY$  is the output of the neural network in the last iteration process. The input is  $X = [x_1, x_2, \dots, x_k]^T \in R^{k \times 1}$ . The feedback weight is  $W_r = [W_{r1}, W_{r2}, \dots, W_{rk}]^T \in R^{k \times 1}$ .

Because the second input layer and the third input layer only play a role of transmission, and do not carry out other processing. So the output of the two input layers is unchanged. The output is  $Y^1 = [y_1^1, y_2^1, \dots, y_k^1]^T \in R^{k \times 1}$ .

**Layer 2-Membership layer:** In this layer, each node is a membership function that usually selects Gaussian function to realize the fuzzification operation, enhancing the ability of neural network to deal with nonlinearity.  $u = [u_1^1, u_2^1, \dots, u_L^1, u_1^2, u_2^2, \dots, u_L^2, \dots, u_1^k, u_2^k, \dots, u_L^k]^T \in R^{kL \times 1}$ , where  $u_j^i$  represents the  $j$ -th Gaussian function of the  $i$ -th input layer node, expressed as:

$$y_{ij}^2 = u_j^i = \exp\left[-\frac{(y_i^1 + r_{ij} \cdot exu_j^i - m_j^i)^2}{(\sigma_j^i)^2}\right] \quad (i = 1, 2, \dots, k; j = 1, 2, \dots, L) \quad (17)$$

where  $M = [m_1^1, m_2^1, \dots, m_L^1, m_1^2, m_2^2, \dots, m_L^2, \dots, m_1^k, m_2^k, \dots, m_L^k]^T \in R^{kL \times 1}$  is the center. The base width is

$$\sigma = [\sigma_1^1, \sigma_2^1, \dots, \sigma_L^1, \sigma_1^2, \sigma_2^2, \dots, \sigma_L^2, \dots, \sigma_1^k, \sigma_2^k, \dots, \sigma_L^k]^T \in R^{kL \times 1};$$

$$R = [r_1^1, r_2^1, \dots, r_L^1, r_1^2, r_2^2, \dots, r_L^2, \dots, r_1^k, r_2^k, \dots, r_L^k]^T \in R^{kL \times 1}$$

is the feedback weight and  $exu_j^i$  is the output of the membership layer in the last iteration process. The superscript

represents the  $i$ -th input layer and the subscript represents the  $j$ -th Gaussian function.

Finally, the output of the membership layer is given as:

$$Y^2 = [y_1^1, y_2^1, \dots, y_L^1, y_1^2, y_2^2, \dots, y_L^2, \dots, y_1^k, y_2^k, \dots, y_L^k]^T \in R^{kL \times 1}.$$

**Layer 3-Rule layer:** The nodes in the rule layer play the role of preprocessing fuzzy rules. The output of the  $i$ -th node in the rule layer can be expressed as:

$$y_j^3 = \frac{\prod_{i=1}^k y_{ij}^2}{\sum_{j=1}^L \sum_{i=1}^k y_{ij}^2} \quad (i = 1, 2, \dots, k; j = 1, 2, \dots, L) \quad (18)$$

The output is expressed as:  $Y^3 = [y_1^3, y_2^3, \dots, y_L^3]^T \in R^{L \times 1}$

**Layer 4-The first hidden layer:** It is a nonlinear activation function, which completes the preliminary feature extraction. The activation function is usually a Gaussian activation function. The output of the  $j$ -th node of the first hidden layer is expressed as:

$$y_j^4 = \phi_{1j} = \exp\left[-\frac{\sum_{i=1}^k (y_i^3 - c_{1j})^2}{(b_{1j})^2}\right], \quad (j = 1, 2, \dots, n) \quad (19)$$

where the center is  $C_1 = [c_{11}, c_{12}, \dots, c_{1n}]^T \in R^{n \times 1}$ , the base width is  $B_1 = [b_{11}, b_{12}, \dots, b_{1n}]^T \in R^{n \times 1}$ , the output is  $Y^4 = [y_1^4, y_2^4, \dots, y_n^4]^T \in R^{n \times 1}$ .

**Layer 5-The second hidden layer:** The second hidden layer completes the further extraction of features, which can improve the accuracy and reduce the computational complexity. The output of the second hidden layer can be expressed as:

$$y_j^5 = \phi_{2j} = \exp\left[-\frac{\sum_{i=1}^k (y_i^4 - c_{2j})^2}{(b_{2j})^2}\right] \quad (20)$$

The center is:  $C_2 = [c_{21}, c_{22}, \dots, c_{2L}]^T \in R^{L \times 1}$ , the base width is:  $B_2 = [b_{21}, b_{22}, \dots, b_{2L}]^T \in R^{L \times 1}$ , the output is:  $Y^5 = [y_1^5, y_2^5, \dots, y_L^5]^T \in R^{L \times 1}$

**Layer 6-Consequent layer:** We use the product of the output of the fuzzy neural network and the double hidden layer neural network as the output of the consequent layer. Therefore, the following expression can be obtained as:

$$y_j^6 = y_j^5 \cdot y_j^3, \quad (j = 1, 2, \dots, L) \quad (21)$$

The output is expressed as:  $Y^6 = G = [y_1^6, y_2^6, \dots, y_L^6]^T \in R^{L \times 1}$

**Layer 7-Output layer:** The output of the previous layer is weighted, and the sum is the final output value of the whole neural network. Its output can be expressed as:

$$Y = W^T G = W_1 y_1^6 + W_2 y_2^6 + \dots + W_L y_L^6 \quad (22)$$

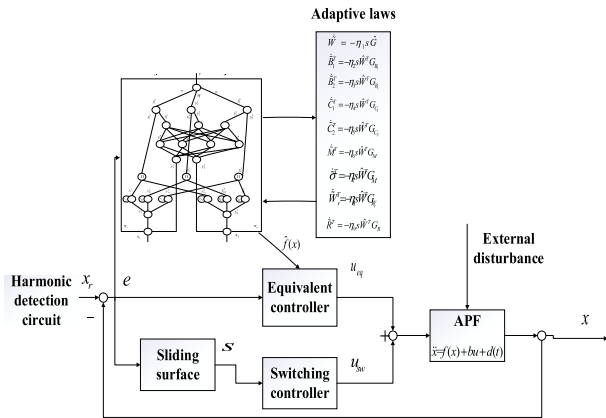


FIGURE 3. The block diagram of FMHLNSMCMFL.

**B. PARAMETER LEARNING OF FMHLNSMCMFL**

Fig.3 is the block diagram of FMHLNSMCMFL. Based on the optimal approximation ability, according to the above neural network, we can obtain the following results:

$$\begin{aligned}
 f(x) &= f^*(x)(s, W_r^*, M^*, \sigma^*, C_1^*, B_1^*, C_2^*, B_2^*, W^*, R^*) + \varepsilon \\
 &= W^{*T} G^*(s, W_r^*, M^*, \sigma^*, C_1^*, B_1^*, C_2^*, B_2^*, W^*, R^*) + \varepsilon
 \end{aligned} \tag{23}$$

where  $\varepsilon$  is the error between the optimal value and the actual value, and  $W_r^*, M^*, \sigma^*, C_1^*, B_1^*, C_2^*, B_2^*, W^*, R^*$  are the best parameters as:

$$\begin{aligned}
 (W_r^*, M^*, \sigma^*, C_1^*, B_1^*, C_2^*, B_2^*, W^*, R^*) \\
 \equiv \arg \min_{(W_r, M, \sigma, C_1, B_1, C_2, B_2, W, R)} [\sup \|f(x) - f^*(x)\|]
 \end{aligned} \tag{24}$$

The output of fuzzy neural network is used to replace the  $f(x)$ , supposed to be:

$$\hat{f}(x) = \hat{W}^T \hat{G}(\hat{W}_r, \hat{M}, \hat{\sigma}, \hat{C}_1, \hat{B}_1, \hat{C}_2, \hat{B}_2, \hat{R}) \tag{25}$$

whew  $\hat{W}_r, \hat{M}, \hat{\sigma}, \hat{C}_1, \hat{B}_1, \hat{C}_2, \hat{B}_2, \hat{W}, \hat{R}$  are estimated values.

Therefore, the difference between the actual value and the estimated value is calculated as:

$$\begin{aligned}
 f(x) - \hat{f}(x) &= W^{*T} G^* - \hat{W}^T \hat{G} + \varepsilon \\
 &= W^{*T} (\hat{G} + G) - \hat{W}^T \hat{G} + \varepsilon \\
 &= W^{*T} \hat{G} + W^{*T} \tilde{G} - \hat{W}^T \hat{G} + \varepsilon \\
 &= (\hat{W}^T + \tilde{W}^T) \hat{G} + (\hat{W}^T + \tilde{W}^T) \tilde{G} - \hat{W}^T \hat{G} + \varepsilon \\
 &= \tilde{W}^T \hat{G} + \hat{W}^T \tilde{G} + \varepsilon_0
 \end{aligned} \tag{26}$$

where the total integral approximation error is:

$$\varepsilon_0 = \tilde{W}^T \tilde{G} + \varepsilon \tag{27}$$

The parameter error is defined as:

$$\tilde{W} = W^* - \hat{W} \tag{28}$$

By expanding Taylor  $G^*$  at  $W_r^* = \hat{W}_r, M^* = \hat{M}, \sigma^* = \hat{\sigma}$ ,

$$C_1^* = \hat{C}_1, B_1^* = \hat{B}_1, C_2^* = \hat{C}_2, B_2^* = \hat{B}_2, R^* = \hat{R},$$

we can get the following results:

$$\begin{aligned}
 &G^*(W_r^*, M^*, \sigma^*, C_1^*, B_1^*, C_2^*, B_2^*, R^*) \\
 &= \hat{G}(\hat{W}_r, \hat{M}, \hat{\sigma}, \hat{C}_1, \hat{B}_1, \hat{C}_2, \hat{B}_2, \hat{R}) + \left. \frac{\partial G}{\partial C_1^*} \right|_{C_1^* = \hat{C}_1} (C_1^* - \hat{C}_1) \\
 &+ \left. \frac{\partial G}{\partial B_1^*} \right|_{B_1^* = \hat{B}_1} (B_1^* - \hat{B}_1) + \left. \frac{\partial G}{\partial C_2^*} \right|_{C_2^* = \hat{C}_2} (C_2^* - \hat{C}_2) \\
 &+ \left. \frac{\partial G}{\partial B_2^*} \right|_{B_2^* = \hat{B}_2} (B_2^* - \hat{B}_2) + \left. \frac{\partial G}{\partial M^*} \right|_{M^* = \hat{M}} (M^* - \hat{M}) \\
 &+ \left. \frac{\partial G}{\partial \sigma^*} \right|_{\sigma^* = \hat{\sigma}} (\sigma^* - \hat{\sigma}) + \left. \frac{\partial G}{\partial W_r^*} \right|_{W_r^* = \hat{W}_r} (W_r^* - \hat{W}_r) \\
 &+ \left. \frac{\partial G}{\partial R^*} \right|_{R^* = \hat{R}} (R^* - \hat{R}) + O_h
 \end{aligned} \tag{29}$$

$$\begin{aligned}
 &\tilde{G}(\tilde{W}_r, \tilde{M}, \tilde{\sigma}, \tilde{C}_1, \tilde{B}_1, \tilde{C}_2, \tilde{B}_2, \tilde{R}) \\
 &= G_{W_r} \cdot \tilde{W}_r + G_M \cdot \tilde{M} + G_\sigma \cdot \tilde{\sigma} + G_R \cdot \tilde{R} \\
 &+ G_{C_1} \cdot \tilde{C}_1 + G_{B_1} \cdot \tilde{B}_1 + G_{C_2} \cdot \tilde{C}_2 + G_{B_2} \cdot \tilde{B}_2 + O_h
 \end{aligned} \tag{30}$$

where  $G_{C_1}, G_{B_1}, G_{C_2}, G_{B_2}, G_M, G_\sigma, G_{W_r}, G_R$  are the partial derivative of  $C_1^*, B_1^*, C_2^*, B_2^*, M^*, \sigma^*, W_r^*, R^*$ , expressed as (31)–(34), shown at the bottom of the next page, (35)–(37), shown at the bottom of page 7, and (38), shown at the bottom of page 8.

Therefore, the estimation error can be written as:

$$\begin{aligned}
 f(x) - \hat{f}(x) \\
 &= \tilde{W}^T \hat{G} + \hat{W}^T \tilde{G} + \varepsilon_0 \\
 &= \tilde{W}^T \hat{G} + \hat{W}^T G_{W_r} \tilde{W}_r + \hat{W}^T G_M \tilde{M} + \hat{W}^T G_\sigma \tilde{\sigma} + \hat{W}^T G_R \tilde{R} \\
 &+ \hat{W}^T G_{C_1} \tilde{C}_1 + \hat{W}^T G_{B_1} \tilde{B}_1 + \hat{W}^T G_{C_2} \tilde{C}_2 \\
 &+ \hat{W}^T G_{B_2} \tilde{B}_2 + \Delta_0
 \end{aligned} \tag{39}$$

where

$$\begin{aligned}
 \Delta_0 &= \hat{W}^T O_h + \varepsilon_0 \\
 &= \hat{W}^T O_h + \tilde{W}^T \tilde{G} + \varepsilon
 \end{aligned} \tag{40}$$

$\Delta_0$  is the total integral higher order approximation error, and we assume that the following inequality holds:

$$|\Delta_0| \leq \bar{\Delta}_d \tag{41}$$

where  $\bar{\Delta}_d$  is a positive constant.

**C. STABILITY ANALYSIS**

The control law of the proposed FMHLNSMCMFL can be expressed as:

$$\begin{aligned}
 u &= \hat{u}_{eq} + u_{sw} \\
 &= -\frac{1}{b} [-\ddot{x}_r + c\dot{e} + \hat{f}(x) + K_w \text{sgn}(s)]
 \end{aligned} \tag{42}$$

*Theorem 2:* Considering the nonlinear mathematical model (6), if we choose the controller (42), the asymptotic stability of APF control system can be guaranteed.

*Proof:* For the proposed FMHLNSMCMFL, we define a new Lyapunov function candidate as:

$$V = \frac{1}{2}s^2 + \frac{1}{2\eta_1}\tilde{W}^T\tilde{W} + \frac{1}{2\eta_2}\tilde{B}_1^T\tilde{B}_1 + \frac{1}{2\eta_3}\tilde{B}_2^T\tilde{B}_2 + \frac{1}{2\eta_4}\tilde{C}_1^T\tilde{C}_1 + \frac{1}{2\eta_5}\tilde{C}_2^T\tilde{C}_2 + \frac{1}{2\eta_6}\tilde{M}^T\tilde{M} + \frac{1}{2\eta_7}\tilde{\sigma}^T\tilde{\sigma} + \frac{1}{2\eta_8}\tilde{W}_r^T\tilde{W}_r + \frac{1}{2\eta_9}\tilde{R}^T\tilde{R} \quad (43)$$

Substituting (10) and (13) into the first derivative of the Lyapunov function (43), and then making

$$H = \frac{1}{\eta_1}\dot{\tilde{W}}^T\tilde{W} + \frac{1}{\eta_2}\dot{\tilde{B}}_1^T\tilde{B}_1 + \frac{1}{\eta_3}\dot{\tilde{B}}_2^T\tilde{B}_2 + \frac{1}{\eta_4}\dot{\tilde{C}}_1^T\tilde{C}_1 + \frac{1}{\eta_5}\dot{\tilde{C}}_2^T\tilde{C}_2 + \frac{1}{\eta_6}\dot{\tilde{M}}^T\tilde{M} + \frac{1}{\eta_7}\dot{\tilde{\sigma}}^T\tilde{\sigma} + \frac{1}{\eta_8}\dot{\tilde{W}}_r^T\tilde{W}_r + \frac{1}{\eta_9}\dot{\tilde{R}}^T\tilde{R} \quad (44)$$

We can obtain:

$$\begin{aligned} \dot{V} &= s\dot{s} + H \\ &= s(c\dot{e} + \ddot{e}) + H \\ &= s(c\dot{e} + f(x) + bu + d - \ddot{x}_r) + H \\ &= s[c\dot{e} + f(x) - u_{eq} - K_w \text{sgn}(s) + d - \ddot{x}_r] + H \end{aligned} \quad (45)$$

Substituting equation (42) into (45), we can get:

$$\begin{aligned} \dot{V} &= s[c\dot{e} + f(x) - u_{eq} - K_w \text{sgn}(s) + d - \ddot{x}_r + bu - bu] + H \\ &= s\{c\dot{e} + f(x) - u_{eq} - K_w \text{sgn}(s) + d - \ddot{x}_r \\ &\quad + b[-\frac{1}{b}(-\ddot{x}_r + c\dot{e} + f(x)) - b[-\frac{1}{b}(-\ddot{x}_r + c\dot{e} + \hat{f}(x)) \\ &\quad - K_w \text{sgn}(s)]\} + H \\ &= s(\hat{f}(x) - f(x) - K_w \text{sgn}(s) + d) + H \end{aligned}$$

$$G_{C_1} = \left. \frac{\partial G^*}{\partial C_1^{*T}} \right|_{C_1^* = \hat{C}_1} = \begin{bmatrix} \frac{\partial y_1^6}{\partial C_1^T} \\ \frac{\partial y_2^6}{\partial C_1^T} \\ \vdots \\ \frac{\partial y_L^6}{\partial C_1^T} \end{bmatrix} = \begin{bmatrix} \frac{\partial y_1^6}{\partial c_{11}} & \frac{\partial y_1^6}{\partial c_{12}} & \cdots & \frac{\partial y_1^6}{\partial c_{1n}} \\ \frac{\partial y_2^6}{\partial c_{11}} & \frac{\partial y_2^6}{\partial c_{12}} & \cdots & \frac{\partial y_2^6}{\partial c_{1n}} \\ \vdots & \vdots & \ddots & \vdots \\ \frac{\partial y_L^6}{\partial c_{11}} & \frac{\partial y_L^6}{\partial c_{12}} & \cdots & \frac{\partial y_L^6}{\partial c_{1n}} \end{bmatrix}_{L \times n} \quad (31)$$

$$G_{B_1} = \left. \frac{\partial G^*}{\partial B_1^{*T}} \right|_{B_1^* = \hat{B}_1} = \begin{bmatrix} \frac{\partial y_1^6}{\partial B_1^T} \\ \frac{\partial y_2^6}{\partial B_1^T} \\ \vdots \\ \frac{\partial y_L^6}{\partial B_1^T} \end{bmatrix} = \begin{bmatrix} \frac{\partial y_1^6}{\partial b_{11}} & \frac{\partial y_1^6}{\partial b_{12}} & \cdots & \frac{\partial y_1^6}{\partial b_{1n}} \\ \frac{\partial y_2^6}{\partial b_{11}} & \frac{\partial y_2^6}{\partial b_{12}} & \cdots & \frac{\partial y_2^6}{\partial b_{1n}} \\ \vdots & \vdots & \ddots & \vdots \\ \frac{\partial y_L^6}{\partial b_{11}} & \frac{\partial y_L^6}{\partial b_{12}} & \cdots & \frac{\partial y_L^6}{\partial b_{1n}} \end{bmatrix}_{L \times n} \quad (32)$$

$$G_{C_2} = \left. \frac{\partial G^*}{\partial C_2^{*T}} \right|_{C_2^* = \hat{C}_2} = \begin{bmatrix} \frac{\partial y_1^6}{\partial C_2^T} \\ \frac{\partial y_2^6}{\partial C_2^T} \\ \vdots \\ \frac{\partial y_L^6}{\partial C_2^T} \end{bmatrix} = \begin{bmatrix} \frac{\partial y_1^6}{\partial c_{21}} & \frac{\partial y_1^6}{\partial c_{22}} & \cdots & \frac{\partial y_1^6}{\partial c_{2L}} \\ \frac{\partial y_2^6}{\partial c_{21}} & \frac{\partial y_2^6}{\partial c_{22}} & \cdots & \frac{\partial y_2^6}{\partial c_{2L}} \\ \vdots & \vdots & \ddots & \vdots \\ \frac{\partial y_L^6}{\partial c_{21}} & \frac{\partial y_L^6}{\partial c_{22}} & \cdots & \frac{\partial y_L^6}{\partial c_{2L}} \end{bmatrix}_{L \times L} \quad (33)$$

$$G_{B_2} = \left. \frac{\partial G^*}{\partial B_2^{*T}} \right|_{B_2^* = \hat{B}_2} = \begin{bmatrix} \frac{\partial y_1^6}{\partial B_2^T} \\ \frac{\partial y_2^6}{\partial B_2^T} \\ \vdots \\ \frac{\partial y_L^6}{\partial B_2^T} \end{bmatrix} = \begin{bmatrix} \frac{\partial y_1^6}{\partial b_{21}} & \frac{\partial y_1^6}{\partial b_{22}} & \cdots & \frac{\partial y_1^6}{\partial b_{2L}} \\ \frac{\partial y_2^6}{\partial b_{21}} & \frac{\partial y_2^6}{\partial b_{22}} & \cdots & \frac{\partial y_2^6}{\partial b_{2L}} \\ \vdots & \vdots & \ddots & \vdots \\ \frac{\partial y_L^6}{\partial b_{21}} & \frac{\partial y_L^6}{\partial b_{22}} & \cdots & \frac{\partial y_L^6}{\partial b_{2L}} \end{bmatrix}_{L \times L} \quad (34)$$



$$\begin{aligned}
 &= s[\tilde{W}^T \hat{G} + \hat{W}^T G_{C_1} \tilde{C}_1 + \hat{W}^T G_{B_1} \tilde{B}_1 + \hat{W}^T G_{C_2} \tilde{C}_2 \\
 &\quad + \hat{W}^T G_{B_2} \tilde{B}_2 + \hat{W}^T G_M \tilde{M} \\
 &\quad + \hat{W}^T G_\sigma \tilde{\sigma} + \hat{W}^T G_{W_r} \tilde{W}_r + \hat{W}^T G_{R\tilde{R}} + \Delta_0 \\
 &\quad - K_w \text{sgn}(s+d)] + H
 \end{aligned} \tag{46}$$

Substituting equation (44) into (46), we can obtain:

$$\begin{aligned}
 \dot{V} = & s[\tilde{W}^T \hat{G} + \hat{W}^T G_{C_1} \tilde{C}_1 + \hat{W}^T G_{B_1} \tilde{B}_1 + \hat{W}^T G_{C_2} \tilde{C}_2 + \hat{W}^T G_{B_2} \tilde{B}_2 \\
 & + \hat{W}^T G_M \tilde{M} + \hat{W}^T G_\sigma \tilde{\sigma} + \hat{W}^T G_{W_r} \tilde{W}_r + \hat{W}^T G_{R\tilde{R}} + \Delta_0 \\
 & - K_w \text{sgn}(s+d)] + \frac{1}{\eta_1} \dot{\tilde{W}}^T \tilde{W} + \frac{1}{\eta_2} \dot{\tilde{B}}_1^T \tilde{B}_1 + \frac{1}{\eta_3} \dot{\tilde{B}}_2^T \tilde{B}_2
 \end{aligned} \tag{35}$$

$$\begin{aligned}
 G_M &= \left. \frac{\partial G^*}{\partial M^{*T}} \right|_{M^*=\hat{M}} = \begin{bmatrix} \frac{\partial y_1^6}{\partial M^{*T}} \\ \frac{\partial y_2^6}{\partial M^{*T}} \\ \vdots \\ \frac{\partial y_L^6}{\partial M^{*T}} \end{bmatrix}_{L \times 1} \\
 &= \begin{bmatrix} \frac{\partial y_1^6}{\partial m_1^1} & \frac{\partial y_1^6}{\partial m_2^1} & \cdots & \frac{\partial y_1^6}{\partial m_L^1} & \frac{\partial y_1^6}{\partial m_1^2} & \frac{\partial y_1^6}{\partial m_2^2} & \frac{\partial y_1^6}{\partial m_L^2} & \cdots & \frac{\partial y_1^6}{\partial m_1^k} & \frac{\partial y_1^6}{\partial m_2^k} & \cdots & \frac{\partial y_1^6}{\partial m_L^k} \\ \frac{\partial y_2^6}{\partial m_1^1} & \frac{\partial y_2^6}{\partial m_2^1} & \cdots & \frac{\partial y_2^6}{\partial m_L^1} & \frac{\partial y_2^6}{\partial m_1^2} & \frac{\partial y_2^6}{\partial m_2^2} & \frac{\partial y_2^6}{\partial m_L^2} & \cdots & \frac{\partial y_2^6}{\partial m_1^k} & \frac{\partial y_2^6}{\partial m_2^k} & \cdots & \frac{\partial y_2^6}{\partial m_L^k} \\ \vdots & \vdots & \ddots & \vdots & \vdots & \vdots & \vdots & \ddots & \vdots & \vdots & \ddots & \vdots \\ \frac{\partial y_L^6}{\partial m_1^1} & \frac{\partial y_L^6}{\partial m_2^1} & \cdots & \frac{\partial y_L^6}{\partial m_L^1} & \frac{\partial y_L^6}{\partial m_1^2} & \frac{\partial y_L^6}{\partial m_2^2} & \frac{\partial y_L^6}{\partial m_L^2} & \cdots & \frac{\partial y_L^6}{\partial m_1^k} & \frac{\partial y_L^6}{\partial m_2^k} & \cdots & \frac{\partial y_L^6}{\partial m_L^k} \end{bmatrix}_{L \times kL}
 \end{aligned} \tag{35}$$

$$\begin{aligned}
 G_\sigma &= \left. \frac{\partial G^*}{\partial \sigma^{*T}} \right|_{\sigma^*=\hat{\sigma}} = \begin{bmatrix} \frac{\partial y_1^6}{\partial \sigma^{*T}} \\ \frac{\partial y_2^6}{\partial \sigma^{*T}} \\ \vdots \\ \frac{\partial y_L^6}{\partial \sigma^{*T}} \end{bmatrix}_{L \times 1} \\
 &= \begin{bmatrix} \frac{\partial y_1^6}{\partial \sigma_1^1} & \frac{\partial y_1^6}{\partial \sigma_2^1} & \cdots & \frac{\partial y_1^6}{\partial \sigma_L^1} & \frac{\partial y_1^6}{\partial \sigma_1^2} & \frac{\partial y_1^6}{\partial \sigma_2^2} & \frac{\partial y_1^6}{\partial \sigma_L^2} & \cdots & \frac{\partial y_1^6}{\partial \sigma_1^k} & \frac{\partial y_1^6}{\partial \sigma_2^k} & \cdots & \frac{\partial y_1^6}{\partial \sigma_L^k} \\ \frac{\partial y_2^6}{\partial \sigma_1^1} & \frac{\partial y_2^6}{\partial \sigma_2^1} & \cdots & \frac{\partial y_2^6}{\partial \sigma_L^1} & \frac{\partial y_2^6}{\partial \sigma_1^2} & \frac{\partial y_2^6}{\partial \sigma_2^2} & \frac{\partial y_2^6}{\partial \sigma_L^2} & \cdots & \frac{\partial y_2^6}{\partial \sigma_1^k} & \frac{\partial y_2^6}{\partial \sigma_2^k} & \cdots & \frac{\partial y_2^6}{\partial \sigma_L^k} \\ \vdots & \vdots & \ddots & \vdots & \vdots & \vdots & \vdots & \ddots & \vdots & \vdots & \ddots & \vdots \\ \frac{\partial y_L^6}{\partial \sigma_1^1} & \frac{\partial y_L^6}{\partial \sigma_2^1} & \cdots & \frac{\partial y_L^6}{\partial \sigma_L^1} & \frac{\partial y_L^6}{\partial \sigma_1^2} & \frac{\partial y_L^6}{\partial \sigma_2^2} & \frac{\partial y_L^6}{\partial \sigma_L^2} & \cdots & \frac{\partial y_L^6}{\partial \sigma_1^k} & \frac{\partial y_L^6}{\partial \sigma_2^k} & \cdots & \frac{\partial y_L^6}{\partial \sigma_L^k} \end{bmatrix}_{L \times kL}
 \end{aligned} \tag{36}$$

$$\begin{aligned}
 G_{W_r} &= \left. \frac{\partial G^*}{\partial W_r^{*T}} \right|_{W_r^*=\hat{W}_r} = \begin{bmatrix} \frac{\partial y_1^6}{\partial W_r^T} \\ \frac{\partial y_2^6}{\partial W_r^T} \\ \vdots \\ \frac{\partial y_L^6}{\partial W_r^T} \end{bmatrix} = \begin{bmatrix} \frac{\partial y_1^6}{\partial W_{r1}^T} & \frac{\partial y_1^6}{\partial W_{r2}^T} & \cdots & \frac{\partial y_1^6}{\partial W_{rk}^T} \\ \frac{\partial y_2^6}{\partial W_{r1}^T} & \frac{\partial y_2^6}{\partial W_{r2}^T} & \cdots & \frac{\partial y_2^6}{\partial W_{rk}^T} \\ \vdots & \vdots & \ddots & \vdots \\ \frac{\partial y_L^6}{\partial W_{r1}^T} & \frac{\partial y_L^6}{\partial W_{r2}^T} & \cdots & \frac{\partial y_L^6}{\partial W_{rk}^T} \end{bmatrix}_{L \times k}
 \end{aligned} \tag{37}$$

$$\begin{aligned}
 & + \frac{1}{\eta_4} \dot{\tilde{C}}_1^T \tilde{C}_1 \\
 & + \frac{1}{\eta_5} \dot{\tilde{C}}_2^T \tilde{C}_2 + \frac{1}{\eta_6} \dot{\tilde{M}}^T \tilde{M} + \frac{1}{\eta_7} \dot{\tilde{\sigma}}^T \tilde{\sigma} + \frac{1}{\eta_8} \dot{\tilde{W}}_r^T \tilde{W}_r + \frac{1}{\eta_9} \dot{\tilde{R}}^T \tilde{R} \\
 = & (s\tilde{W}^T \hat{G} + \frac{1}{\eta_1} \dot{\tilde{W}}^T \tilde{W}) + (s\hat{W}^T G_{B_1} \tilde{B}_1 + \frac{1}{\eta_2} \dot{\tilde{B}}_1^T \tilde{B}_1) \\
 & + (s\hat{W}^T G_{B_2} \tilde{B}_2 + \frac{1}{\eta_3} \dot{\tilde{B}}_2^T \tilde{B}_2) \\
 & + (s\hat{W}^T G_{C_1} \tilde{C}_1 + \frac{1}{\eta_4} \dot{\tilde{C}}_1^T \tilde{C}_1) \\
 & + (s\hat{W}^T G_{C_2} \tilde{C}_2 + \frac{1}{\eta_5} \dot{\tilde{C}}_2^T \tilde{C}_2) + (s\hat{W}^T G_M \tilde{M} + \frac{1}{\eta_6} \dot{\tilde{M}}^T \tilde{M}) \\
 & + (s\hat{W}^T G_\sigma \tilde{\sigma} + \frac{1}{\eta_7} \dot{\tilde{\sigma}}^T \tilde{\sigma}) + (s\hat{W}^T G_{W_r} \tilde{W}_r + \frac{1}{\eta_8} \dot{\tilde{W}}_r^T \tilde{W}_r) \\
 & + (s\hat{W}^T G_R \tilde{R} + \frac{1}{\eta_9} \dot{\tilde{R}}^T \tilde{R}) \\
 & + \Delta_0 - K_w \text{sgn}(s) + d \tag{47}
 \end{aligned}$$

So the following adaptive laws are selected:

Let  $s\tilde{W}^T \hat{G} + \frac{1}{\eta_1} \dot{\tilde{W}}^T \tilde{W} = 0$ , we can obtain:

$$\dot{\tilde{W}} = -\eta_1 s \hat{G} \tag{48}$$

Let  $s\hat{W}^T G_{B_1} \tilde{B}_1 + \frac{1}{\eta_2} \dot{\tilde{B}}_1^T \tilde{B}_1 = 0$ , we can obtain:

$$\dot{\tilde{B}}_1^T = -\eta_2 s \hat{W}^T G_{B_1} \tag{49}$$

Let  $s\hat{W}^T G_{B_2} \tilde{B}_2 + \frac{1}{\eta_3} \dot{\tilde{B}}_2^T \tilde{B}_2 = 0$ , we can obtain:

$$\dot{\tilde{B}}_2^T = -\eta_3 s \hat{W}^T G_{B_2} \tag{50}$$

Let  $s\hat{W}^T G_{C_1} \tilde{C}_1 + \frac{1}{\eta_4} \dot{\tilde{C}}_1^T \tilde{C}_1 = 0$ , we can obtain:

$$\dot{\tilde{C}}_1^T = -\eta_4 s \hat{W}^T G_{C_1} \tag{51}$$

Let  $s\hat{W}^T G_{C_2} \tilde{C}_2 + \frac{1}{\eta_5} \dot{\tilde{C}}_2^T \tilde{C}_2 = 0$ , we can obtain:

$$\dot{\tilde{C}}_2^T = -\eta_5 s \hat{W}^T G_{C_2} \tag{52}$$

Let  $s\hat{W}^T G_M \tilde{M} + \frac{1}{\eta_6} \dot{\tilde{M}}^T \tilde{M} = 0$ , we can obtain:

$$\dot{\tilde{M}}^T = -\eta_6 s \hat{W}^T G_M \tag{53}$$

Let  $s\hat{W}^T G_\sigma \tilde{\sigma} + \frac{1}{\eta_7} \dot{\tilde{\sigma}}^T \tilde{\sigma} = 0$ , we can obtain:

$$\dot{\tilde{\sigma}}^T = -\eta_7 s \hat{W}^T G_\sigma \tag{54}$$

Let  $s\hat{W}^T G_{W_r} \tilde{W}_r + \frac{1}{\eta_8} \dot{\tilde{W}}_r^T \tilde{W}_r = 0$ , we can obtain:

$$\dot{\tilde{W}}_r^T = -\eta_8 s \hat{W}^T G_{W_r} \tag{55}$$

Let  $s\hat{W}^T G_R \tilde{R} + \frac{1}{\eta_9} \dot{\tilde{R}}^T \tilde{R} = 0$ , we can obtain:

$$\dot{\tilde{R}}^T = -\eta_9 s \hat{W}^T G_R \tag{56}$$

If the adaptive laws (48-56) are satisfied, we can obtain:

$$\begin{aligned}
 \dot{V} & = -K_w |s| + s(\Delta_0 + d(t)) \\
 & \leq -K_w |s| + \|s\| (\bar{\Delta}_d + D) \\
 & = -|s| (K_w - \bar{\Delta}_d - D) \tag{57}
 \end{aligned}$$

If  $K_w > \bar{\Delta}_d + D$ ,  $\dot{V} \leq 0$ . Integrating  $\dot{V}$  with respect to time, we can get

$$\int_0^t |s| dt \leq \frac{1}{K_w - \bar{\Delta}_d - D} (V(t) - V(0)). \tag{58}$$

Since  $V(0)$  is bounded and  $V(t)$  is nonincreasing, it is concluded that  $\lim_{t \rightarrow \infty} \int_0^t |s| dt$  is bounded. According to Barbalat lemma, one can deduce that  $\lim_{t \rightarrow \infty} s(t) = 0$  and  $\lim_{t \rightarrow \infty} e(t) = 0$ , which means the tracking error and sliding surface will converge to zero asymptotically.

$$\begin{aligned}
 G_R & = \left. \frac{\partial G^*}{\partial R^{*T}} \right|_{R^* = \hat{R}} = \begin{bmatrix} \frac{\partial y_1^6}{\partial R^{*T}} \\ \frac{\partial y_2^6}{\partial R^{*T}} \\ \vdots \\ \frac{\partial y_L^6}{\partial R^{*T}} \end{bmatrix}_{L \times 1} \\
 & = \begin{bmatrix} \frac{\partial y_1^6}{\partial r_{11}} & \frac{\partial y_1^6}{\partial r_{12}} & \cdots & \frac{\partial y_1^6}{\partial r_{1L}} & \frac{\partial y_1^6}{\partial r_{21}} & \frac{\partial y_1^6}{\partial r_{22}} & \cdots & \frac{\partial y_1^6}{\partial r_{2L}} & \cdots & \frac{\partial y_1^6}{\partial r_{k1}} & \frac{\partial y_1^6}{\partial r_{k2}} & \cdots & \frac{\partial y_1^6}{\partial r_{kL}} \\ \frac{\partial y_2^6}{\partial r_{11}} & \frac{\partial y_2^6}{\partial r_{12}} & \cdots & \frac{\partial y_2^6}{\partial r_{1L}} & \frac{\partial y_2^6}{\partial r_{21}} & \frac{\partial y_2^6}{\partial r_{22}} & \cdots & \frac{\partial y_2^6}{\partial r_{2L}} & \cdots & \frac{\partial y_2^6}{\partial r_{k1}} & \frac{\partial y_2^6}{\partial r_{k2}} & \cdots & \frac{\partial y_2^6}{\partial r_{kL}} \\ \vdots & \vdots & \ddots & \vdots & \vdots & \vdots & \ddots & \vdots & \cdots & \vdots & \vdots & \ddots & \vdots \\ \frac{\partial y_L^6}{\partial r_{11}} & \frac{\partial y_L^6}{\partial r_{12}} & \cdots & \frac{\partial y_L^6}{\partial r_{1L}} & \frac{\partial y_L^6}{\partial r_{21}} & \frac{\partial y_L^6}{\partial r_{22}} & \cdots & \frac{\partial y_L^6}{\partial r_{2L}} & \cdots & \frac{\partial y_L^6}{\partial r_{k1}} & \frac{\partial y_L^6}{\partial r_{k2}} & \cdots & \frac{\partial y_L^6}{\partial r_{kL}} \end{bmatrix}_{L \times kL} \tag{38}
 \end{aligned}$$



IV. SIMULATION STUDY

The reliability of the proposed controller was verified by MATLAB/Simulink package with SimPower Toolbox. In the simulation process, the selection of relevant parameters is shown in Table 1.

In MATLAB simulation, the parameters of sliding mode controller are selected as  $c = 15000, K_w = 2e4$ . The parameters in the FMHLNSMCMFL are  $k = 1, L = 2, n = 3$  and learning rates are  $\eta_1 = 2e4, \eta_2 = 0.08, \eta_3 = 0.1, \eta_4 = 0.2, \eta_5 = 0.12, \eta_6 = 0.25, \eta_7 = 0.1, \eta_8 = 0.2, \eta_9 = 0.8$ . In order to verify the effectiveness of the proposed algorithm, an APF harmonic control algorithm using a sliding mode controller with a neural network controller is proposed for comparative study.

TABLE 1. APF model parameters.

Parameters	Values
Supply voltage	$U_s = 24V, f = 50Hz$
Steady load	$R_1 = 5\Omega, R_2 = 15\Omega, C = 1000\mu F$
Dynamic load	$R_1 = 15\Omega, R_2 = 15\Omega, C = 1000\mu F$
APF main circuit parameters	$L_c = 10mH, R_c = 0.1\Omega, C = 2200\mu F, U_{dc}^* = 50V$
Switching frequency	$f_{sw} = 10KHz$
Sampling time	$T_s = 5e^{-5}s$

Fig.4 shows that when  $t = 0s$ , the total current distortion rate is 35.07% without APF compensation. The current distortion effect of the circuit is serious, which could cause great damage to the power grid. Fig.5 shows the source current curve before and after harmonic compensation. After 0.05 seconds, the circuit breaker changes from open to closed, meaning that the main circuit begins to carry out harmonic compensation, and the source current changes from distorted waveform to sinusoidal waveform. When  $t = 0.3s$ , a nonlinear load is paralleled to the power grid, so the total resistance decreases, that is, the amplitude of source current becomes larger. On the contrary, when  $t = 0.6s$ , the amplitude of source current will decrease.

Fig.6 shows the current tracking diagram under the proposed control algorithm. We can see that the current tracking effect is good, and the reference current can be tracked in a short time. The error of reference current and compensation current under two controllers can be seen in Fig.7a and Fig.8a. Fig.7b and Fig.8b are the enlarged diagrams of the Fig.7a and Fig.8a respectively. After harmonic compensation is started, the error tends to 0 in a short time.

In order to control the voltage of the DC side capacitor, a traditional PI controller is adopted, where  $K_p = 0.15$  and  $K_i = 0$ . As can be seen in Fig.9, the DC-side voltage can quickly reach a stable reference value of 50V.

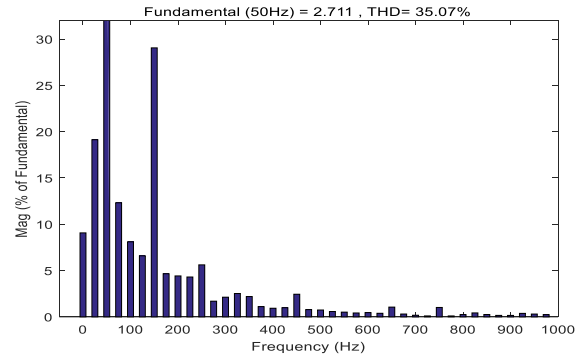


FIGURE 4. Compensated source current spectrum analysis before compensation.

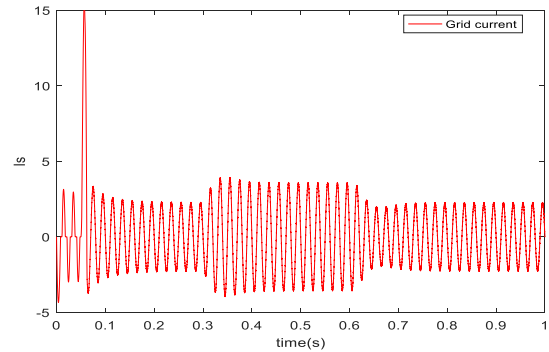
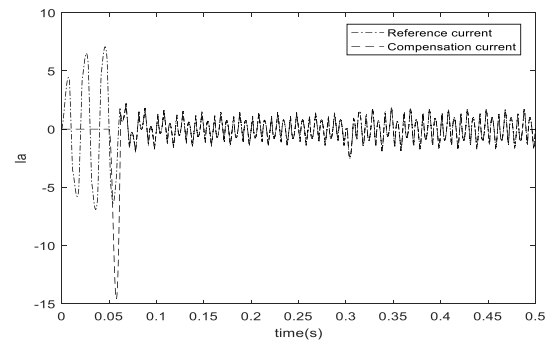
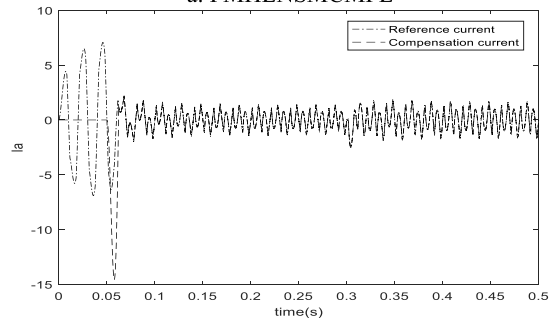


FIGURE 5. Source current curve before and after compensation under FMHLNSMCMFL.



a. FMHLNSMCMFL



b. SMC with NN

FIGURE 6. Harmonic current tracking curve under two controllers.

We measured the THD at  $t = 0.2s, t = 0.4s, t = 0.7s$  using two controllers as shown in Table 2. The THD under the FMHLNSMCMFL method is smaller than the

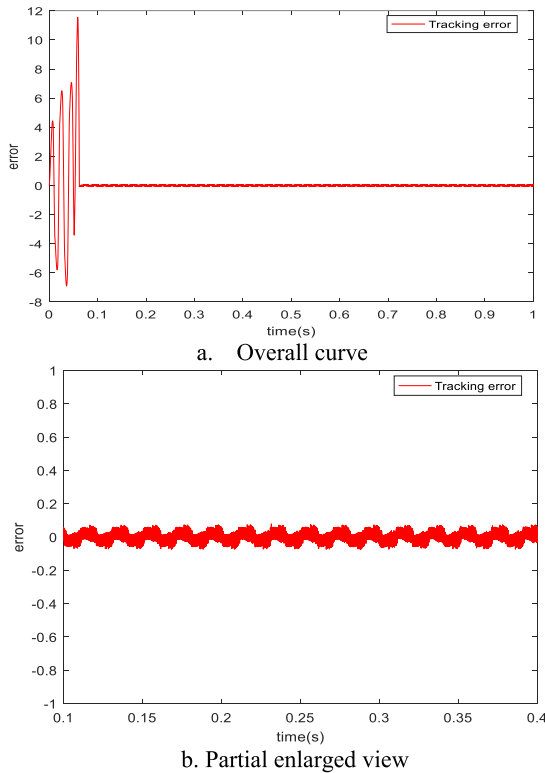


FIGURE 7. Tracking error curve under FMHLNSMCMFL.

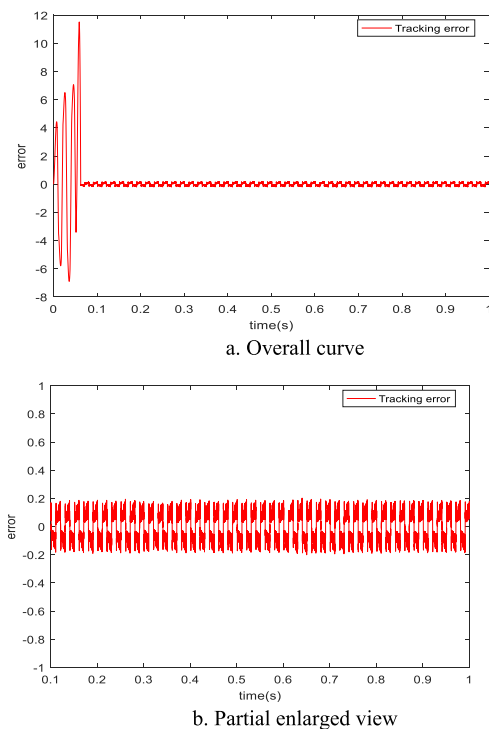


FIGURE 8. Tracking error curve under SMC with NN.

SMC with NN method in all cases, which demonstrates the system performance is greatly improved with the proposed controller.

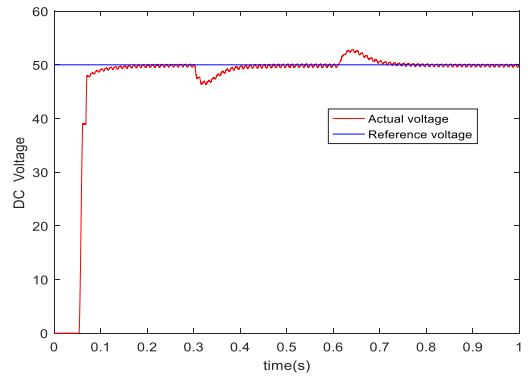


FIGURE 9. DC-side voltage  $U_{dc}$  tracking curve under FMHLNSMCMFL.

Fig.10 is the adaptive parameter curves of each parameter including the base width, weight and center of each layer. These adaptive parameters reflect the online learning ability of our proposed neural network controller, and its adaptive laws are shown in (48)-(56). The proposed neural network controller can update online with the information of the previous state and stabilize to its optimal value with good robustness and self-adjusting ability.

TABLE 2. Comparison of THD value under two controllers.

Method	0s	0.2s	0.4s	0.7s
FMHLNSMCMFL	35.07%	1.62%	1.18%	1.76%
SMC with NN	35.07	2.86%	1.91%	3.25%

## V. REAL-TIME EXPERIMENT STUDY

A prototype was built to verify the validity of the practical application using the proposed controller. Compared with the traditional digital signal processor (DSP), dSPACE runs faster, has a wider input range, and can detect the values of various parameters and variables in real time and draw curves. So we use DS1004 as a prototype control board instead of DSP. According to the structure of the APF in Fig. 1, we can build a single-phase APF prototype as shown in Fig. 11. The prototype mainly includes APF main circuit, power supply, nonlinear load, drive circuit, acquisition circuit, and control board. The transformer is used to convert the mains supply into a 24Vrms AC power as the power supply for the prototype. The main circuit of the single-phase APF consists of four IGBTs, DC-side capacitor, and AC-side inductor. Continuous voltage and current signals are sampled through the sensor. The AD input port of the dSPACE control board receives the collected signal.

In the experiment, the SMC with NN mentioned in the simulation is used as a comparison. The parameters of the prototype are the same as the simulation parameters, which are based on Table 1. The controller parameters also use the same data as in the simulation.

Figs. 12–20 are the experimental results of a single-phase APF prototype. All data are measured using an Agilent InfiniVision 3000X series oscilloscope.

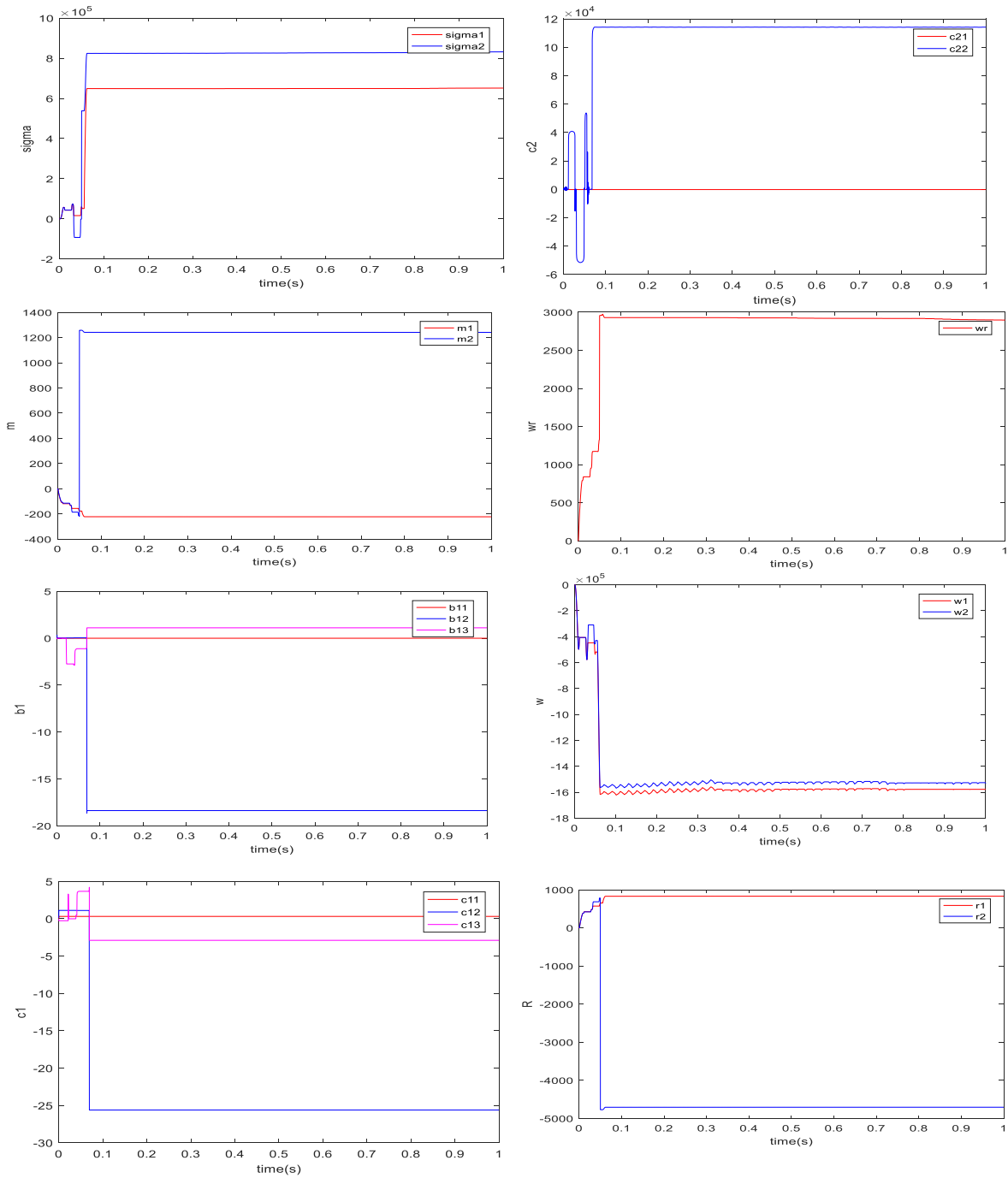


FIGURE 10. Adaptive parameter curve under the proposed FMHLNSMCMFL.

First, we showed the oscilloscope waveform diagram of SMC with NN which shown in Fig. 12. In the oscilloscope, curve 1 (yellow curve) represents the supply voltage, curve 2 (green curve) represents the load current, curve 3 (blue curve) represents the harmonic compensation current, and curve 4 (deep pink curve) represents the grid current. Fig. 12 is the steady-state oscilloscope waveform diagrams using the SMC with NN. The steady-state THD of the system is 4.70%, which is relatively large.

Fig.13 and 14 are the steady-state oscilloscope waveform and THD diagrams using FMHLNSMCMFL. It can be seen in Fig. 13 that when FMHLNSMCMFL used, the grid current quickly returns to a sine wave. Fig. 14 shows that the THD value is 3.89%, which is lower than the value of SMC with NN.

Next, in order to verify the dynamic performance of the system, we paralleled an identical load under the two algorithms and observed its dynamic performance. Fig. 15 is the

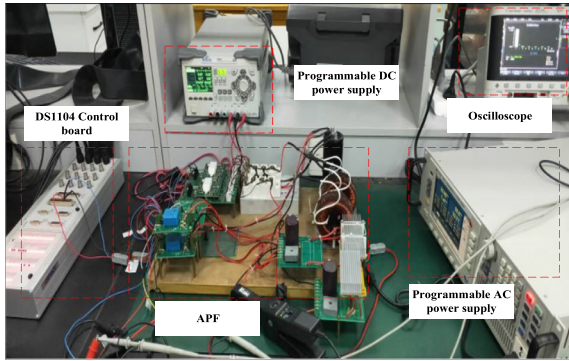


FIGURE 11. Experimental prototype structure.

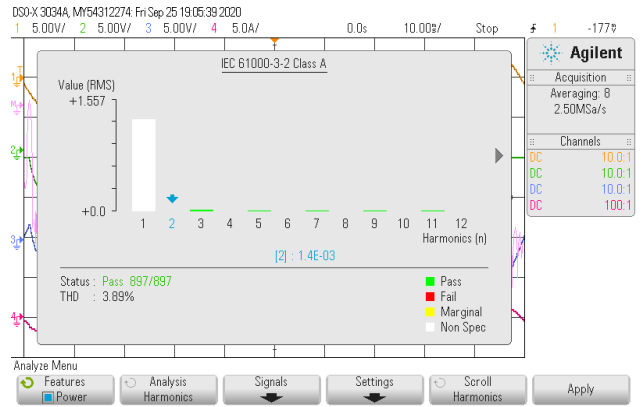


FIGURE 14. Steady-state THD rate under FMHLNSMCMFL.

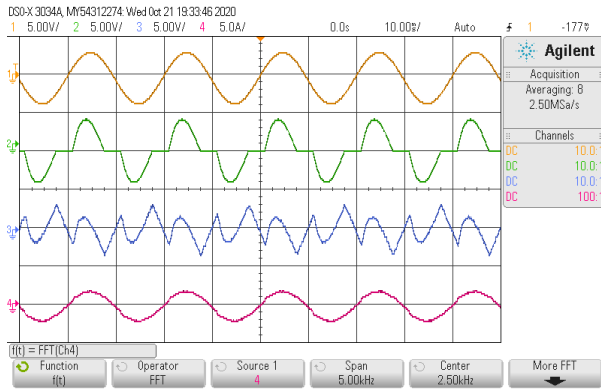


FIGURE 12. Steady-state oscilloscope waveform under SMC with NN.

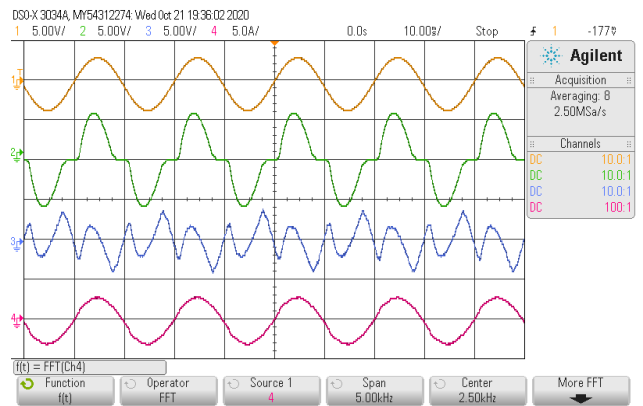


FIGURE 15. Dynamic-state oscilloscope waveform after the load increases under SMC with NN.

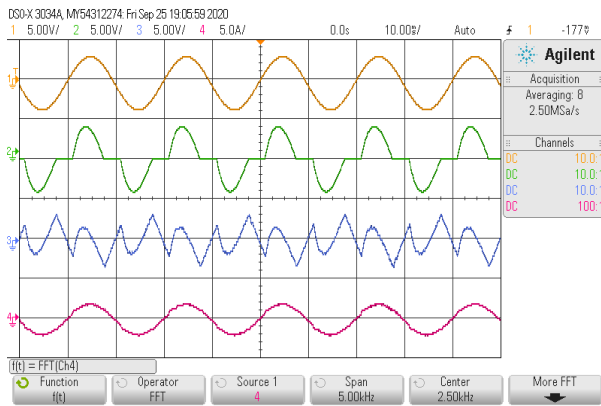


FIGURE 13. Steady-state oscilloscope waveform under FMHLNSMCMFL.

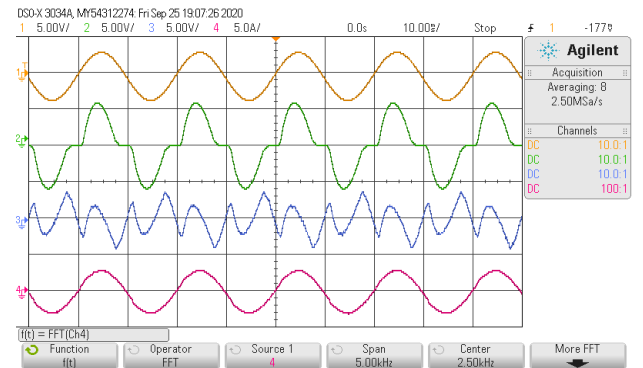


FIGURE 16. Dynamic-state oscilloscope waveform after the load increases under FMHLNSMCMFL.

experimental result of the SMC with NN when the nonlinear load is increased. The system also stabilized at a fast speed and the steady-state THD is 4.23%.

Figs.16 and 17 are the experimental results of FMHLNSMCMFL when the nonlinear load is increased. In Fig. 16, even if the load suddenly increases, the source current (curve 4) can quickly become a sinusoidal waveform, and the THD is 3.4%.

Finally, consider the reduction of nonlinear load. Fig.18 is the experimental results under SMC with NN. The

steady-state THD of the system is 4.72%, which is less than 5%, but it is significantly large. Figs. 19 and 20 show the experimental results when using the FMHLNSMCMFL. In Fig. 20, the grid current power supply quickly returns to a sine wave, and the THD at this time is 3.90%. The data in Table 3 is the current distortion rate. From the above comparative experimental results, the proposed control algorithm not only satisfies the current distortion rate of less than 5%, but also has certain advantages over SMC with NN

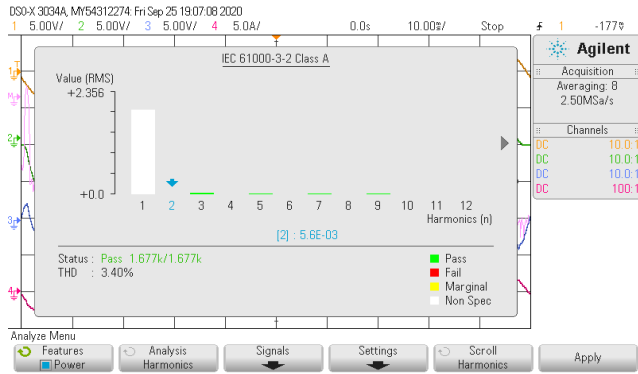


FIGURE 17. Dynamic-state THD rate after the load increases under FMHLNSMCMFL.

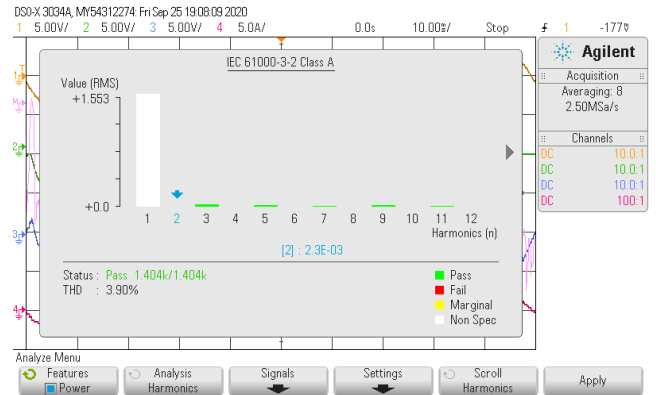


FIGURE 20. Dynamic-state THD rate after the load reduction under FMHLNSMCMFL.

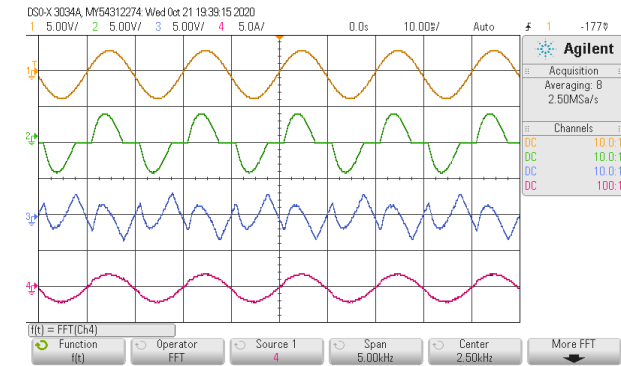


FIGURE 18. Dynamic-state oscilloscope waveform after load reduction under SMC with NN.

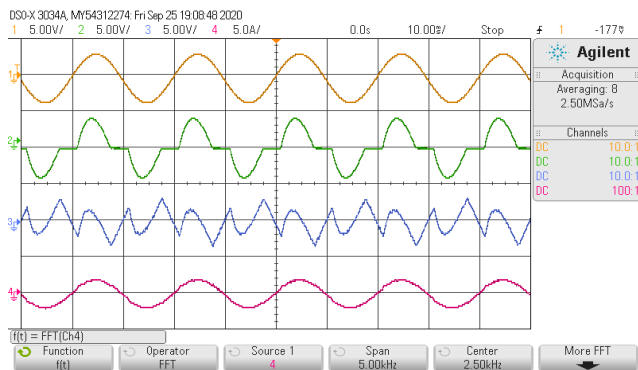


FIGURE 19. Dynamic-state oscilloscope waveform after load reduction under FMHLNSMCMFL.

TABLE 3. Comparison of THD under three controllers.

Method	SMC with NN	FMHLNSMCMFL	FMSCRNN
Steady state	4.70%	3.89%	4.11%
Increase load	4.23%	3.40%	4.46%
Reduce load	4.72%	3.90%	3.91%

in power harmonic compensation. In addition, in Table 3, we have added a set of algorithms currently used for APF harmonic control as a comparison [33]. We can see that

FMHLNSMCMFL is better than this algorithm in both steady state and sudden load conditions.

## VI. CONCLUSION

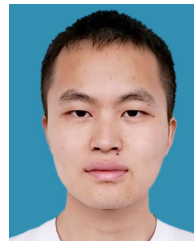
In this paper, a sliding mode control strategy of a single-phase active power filter based on a fuzzy multiple hidden layer neural network with multiple feedback loop is studied. A FMHLNSMCMFL scheme is introduced to approximate the unknown nonlinear term in the dynamic system. The proposed neural network introduces double hidden layers, which reduces the number of nodes while improving accuracy. In addition, the introduction of double feedback also enables the neural network to self-adjust in combination with the state information at the previous moment, improving the approximation ability of the neural network. The simulation and experimental results demonstrate that current tracking error will converge to zero asymptotically, and show that the proposed controller has high compensation accuracy, good dynamic performance and strong robustness. This seemed to be a clear proof of the proposed filter performing well in the harmonic elimination. In the future, in addition to optimizing the structure of the neural network, in-depth research on the adjustment of the learning rate will be carried out to improve the performance of the neural network.

## REFERENCES

- [1] M. A. A. M. Zainuri, A. C. Soh, M. A. M. Radzi, N. A. Rahim, and N. F. A. A. Rahman, "Single phase shunt active power filter with simplified ADALINE neural network," in *Proc. 3rd IET Int. Conf. Clean Energy Technol. (CEAT)*, 2014, pp. 1–6.
- [2] J. H. R. Enslin and P. J. M. Heskes, "Harmonic interaction between a large number of distributed power inverters and the distribution network," *IEEE Trans. Power Electron.*, vol. 19, no. 6, pp. 1586–1593, Nov. 2004.
- [3] R. Martinek, J. Rzidky, R. Jaros, P. Bilik, and M. Ladrova, "Least mean squares and recursive least squares algorithms for total harmonic distortion reduction using shunt active power filter control," *Energies*, vol. 12, no. 8, p. 1545, Apr. 2019.
- [4] Z. Li, L. Wang, Y. Wang, and G. Li, "Harmonic detection method based on adaptive noise cancellation and its application in photovoltaic—Active power filter system," *Electr. Power Syst. Res.*, vol. 184, Jul. 2020, Art. no. 106308.
- [5] T. Platek, "Analysis of ripple current in the capacitors of active power filters," *Energies*, vol. 12, no. 23, p. 4493, Nov. 2019.



- [6] M. B. Ketzer, C. B. Jacobina, and A. M. N. Lima, "Shaping control strategies for active power filters," *IET Power Electron.*, vol. 11, no. 1, pp. 175–181, Jan. 2018.
- [7] K. Wang, Y. Tang, X. Zhang, Y. Wang, C.-J. Zhang, and H. Zhang, "IGBT open-circuit fault diagnosis for 3-phase 4-wire 3-level active power filters based on voltage error correlation," *J. Power Electron.*, vol. 16, no. 5, pp. 1950–1963, Sep. 2016.
- [8] J. Sun and K. Zhao, "Adaptive neural network sliding mode control for active suspension systems with electrohydraulic actuator dynamics," *Int. J. Adv. Robot. Syst.*, vol. 17, no. 4, pp. 1–11, Jul. 2020.
- [9] A. S. Ray and A. Bhattacharya, "Improved tracking of shunt active power filter by sliding mode control," *Int. J. Electr. Power Energy Syst.*, vol. 78, pp. 916–925, Jun. 2016.
- [10] J. Matas, L. G. de Vicuna, J. Miret, J. M. Guerrero, and M. Castilla, "Feedback linearization of a single-phase active power filter via sliding mode control," *IEEE Trans. Power Electron.*, vol. 23, no. 1, pp. 116–125, Jan. 2008.
- [11] M. A. Kouadria, T. Allaoui, and M. Denai, "A hybrid fuzzy sliding-mode control for a three-phase shunt active power filter," *Energy Syst.*, vol. 8, no. 2, pp. 297–308, May 2017.
- [12] A. Haghghi and R. Ziaratban, "A non-integer sliding mode controller to stabilize fractional-order nonlinear systems," *Adv. Difference Equ.*, vol. 2020, no. 1, pp. 211–223, Dec. 2020.
- [13] S. Pashaei and M. A. Badamchizadeh, "Control of a class of fractional-order systems with mismatched disturbances via fractional-order sliding mode controller," *Trans. Inst. Meas. Control*, vol. 42, no. 13, pp. 2423–2439, Sep. 2020.
- [14] Y. Ding, X. Wang, Y. Bai, and N. Cui, "An improved continuous sliding mode controller for flexible air-breathing hypersonic vehicle," *Int. J. Robust Nonlinear Control*, vol. 30, no. 14, pp. 5751–5772, 2020.
- [15] D. Mohammad, R. Behrooz, and R. Noei, "Speed control of switched reluctance motor via fuzzy fast terminal sliding-mode control," *Comput. Electr. Eng.*, vol. 80, pp. 106472–106487, Dec. 2019.
- [16] K. Safa, R. Zahra, and R. Behrooz, "Controlling chaos based on a novel intelligent integral terminal sliding mode control in a rod-type plasma torch," *Chin. Phys. B*, vol. 25, no. 5, pp. 11–22, 2016.
- [17] H. Zhang and Y. Liu, "Adaptive RBF neural network based on sliding mode controller for active power filter," *Int. J. Power Electron.*, vol. 11, no. 4, pp. 460–481, 2020.
- [18] S. Khari, Z. Rahmani, and B. Rezaie, "Designing fuzzy logic controller based on combination of terminal sliding mode and state feedback controllers for stabilizing chaotic behaviour in rod-type plasma torch system," *Trans. Inst. Meas. Control*, vol. 38, no. 2, pp. 150–164, Feb. 2016.
- [19] M. H. Vali, B. Rezaie, and Z. Rahmani, "Designing a neuro-sliding mode controller for networked control systems with packet dropout," *Int. J. Eng.*, vol. 29, pp. 539–548, Apr. 2016.
- [20] X. Fu and S. Li, "Control of single-phase grid-connected converters with LCL filters using recurrent neural network and conventional control methods," *IEEE Trans. Power Electron.*, vol. 31, no. 7, pp. 5354–5364, Jul. 2016.
- [21] J. Fei and Y. Chen, "Dynamic terminal sliding mode control for single-phase active power filter using double hidden layer recurrent neural network," *IEEE Trans. Power Electron.*, vol. 35, no. 9, pp. 9906–9924, Sep. 2020, doi: [10.1109/TPEL.2020.2974470](https://doi.org/10.1109/TPEL.2020.2974470).
- [22] S. Hou, Y. Chu, and J. Fei, "Intelligent global sliding mode control using recurrent feature selection neural network for active power filter," *IEEE Trans. Ind. Electron.*, vol. 68, no. 8, pp. 7320–7329, Aug. 2021, doi: [10.1109/TIE.2020.3000098](https://doi.org/10.1109/TIE.2020.3000098).
- [23] S. Hou, Y. Chu, and J. Fei, "Adaptive type-2 fuzzy neural network inherited terminal sliding mode control for power quality improvement," *IEEE Trans. Ind. Informat.*, vol. 17, no. 11, pp. 7564–7574, Nov. 2021, doi: [10.1109/TII.2021.3049643](https://doi.org/10.1109/TII.2021.3049643).
- [24] J. Fei, Y. Chen, L. Liu, and Y. Fang, "Fuzzy multiple hidden layer recurrent neural control of nonlinear system using terminal sliding-mode controller," *IEEE Trans. Cybern.*, early access, Mar. 12, 2021, doi: [10.1109/TCYB.2021.3052234](https://doi.org/10.1109/TCYB.2021.3052234).
- [25] J. Fei, Z. Wang, X. Liang, Z. Feng, and Y. Xue, "Adaptive fractional sliding mode control of micro gyroscope system using double loop recurrent fuzzy neural network structure," *IEEE Trans. Fuzzy Syst.*, 2021, doi: [10.1109/TFUZZ.2021.3064704](https://doi.org/10.1109/TFUZZ.2021.3064704).
- [26] E. Durna, "Adaptive fuzzy hysteresis band current control for reducing switching losses of hybrid active power filter," *IET Power Electron.*, vol. 11, no. 5, pp. 937–944, May 2018.
- [27] N. Wang and M. J. Er, "Self-constructing adaptive robust fuzzy neural tracking control of surface vehicles with uncertainties and unknown disturbances," *IEEE Trans. Control Syst. Technol.*, vol. 23, no. 3, pp. 991–1002, May 2015.
- [28] S. Hou, Y. Chu, and J. Fei, "Robust intelligent control for a class of power-electronic converters using neuro-fuzzy learning mechanism," *IEEE Trans. Power Electron.*, vol. 36, no. 8, pp. 9441–9452, Aug. 2021, doi: [10.1109/TPEL.2021.3049553](https://doi.org/10.1109/TPEL.2021.3049553).
- [29] J. Fei, H. Wang, and Y. Fang, "Novel neural network fractional-order sliding-mode control with application to active power filter," *IEEE Trans. Syst., Man, Cybern., Syst.*, early access, Apr. 15, 2021, doi: [10.1109/TSMC.2021.3071360](https://doi.org/10.1109/TSMC.2021.3071360).
- [30] P. S. Puhana, P. K. Ray, and G. Panda, "Development of real time implementation of 5/5 rule based fuzzy logic controller shunt active power filter for power quality improvement," *Int. J. Emerg. Electr. Power Syst.*, vol. 17, no. 6, pp. 607–617, Dec. 2016.
- [31] J. Fei and Z. Feng, "Fractional-order finite-time super-twisting sliding mode control of micro gyroscope based on double-loop fuzzy neural network," *IEEE Trans. Syst., Man, Cybern., Syst.*, early access, Mar. 25, 2020, doi: [10.1109/TSMC.2020.2979979](https://doi.org/10.1109/TSMC.2020.2979979).
- [32] J. Fei and Y. Chen, "Fuzzy double hidden layer recurrent neural terminal sliding mode control of single-phase active power filter," *IEEE Trans. Fuzzy Syst.*, early access, Jul. 29, 2020, doi: [10.1109/TFUZZ.2020.3012760](https://doi.org/10.1109/TFUZZ.2020.3012760).
- [33] J. Fei and H. Wang, "Fractional-order adaptive recurrent neural sliding mode control of active power filter," in *Proc. 20th Int. Symp. Power Electron. (Ee)*, Oct. 2019, pp. 1–6, doi: [10.1109/PEE.2019.8923318](https://doi.org/10.1109/PEE.2019.8923318).



**JIE ZHUO** received the B.S. degree in electrical engineering from Hohai University, Changzhou, China, in 2019, where he is currently pursuing the M.S. degree in electrical engineering. His research interests include power electronics, adaptive control, and intelligent control.

**CUICUI AN** received the B.S. and M.S. degrees in mechanical engineering from Hohai University, China, in 2005 and 2008, respectively. She is currently working at Hohai University. Her research interests include mechanical design, nonlinear control, intelligent control, and dynamics and control of mechanical systems.



**JUNTAO FEI** (Senior Member, IEEE) received the B.S. degree in electrical engineering from Hefei University of Technology, China, in 1991, the M.S. degree in electrical engineering from the University of Science and Technology of China, in 1998, and the M.S. and Ph.D. degrees in mechanical engineering from The University of Akron, OH, USA, in 2003 and 2007, respectively. He was a Visiting Scholar with the University of Virginia, VA, USA, a Visiting Scholar at North Carolina State University, Raleigh, NC, USA. He was an Assistant Professor with the University of Louisiana, LA, USA. He is currently a Professor at Hohai University, China, and the Director of the Institute of Electrical and Control Engineering. His research interests include adaptive control, nonlinear control, intelligent control, power electronics, dynamics and control of MEMS, and smart materials and structures.